Lattice vibrational modes of Li_2GeO_3 measured by infrared and Raman techniques

Allen Lurio and Gerald Burns*
IBM Thomas J. Watson Research Center, Yorktown Heights, New York 10598
(Received 24 April 1974)

Li_2GeO_3 is an orthorhombic pyroelectric transparent crystal with space group C_{2v}^{12} ($Cmc2_1$). Scott *et al.* have shown that it can be grown easily in very large boules by the Czochralski technique. We report and discuss infrared reflectivity and Raman measurements of the lattice vibrational modes along all three polarization directions, and the optic index of refraction. The frequencies of the modes determined from the two techniques are in good agreement with each other except that several more modes are observed by the Raman techniques. The clamped-dielectric-constant values calculated from the modes are in fair agreement with our capacitance measurements.

I. INTRODUCTION

Li_2GeO_3 is one member of a class of pyroelectric materials with point group C_{2v}. Recently,[1] it has been shown that large perfect single crystals of this material can be grown easily. The crystal has electromechanical coefficients five times that of α quartz and is one member of a class A_2BO_3, where A = Li, Na and B = Si, Ge which has the pyroelectric orthorhombic space group[2-6] C_{2v}^{12} ($Cmc2_1$). In this paper we report results of polarized infrared and Raman measurements on single crystals of Li_2GeO_3 along the three principal directions of the orthorhombic cell.

II. MODE DETERMINATION

Li_2GeO_3 has a space group $Cmc2_1$ (C_{2v}^{12}) with two molecules per primitive unit cell. The space group shows that the crystal is a member of the orthorhombic crystal system, is pyroelectric with a polarization along the z axis, has a base-centered Bravais lattice (C lattice), and has a glide plane and a screw axis (i.e., is a nonsymorphic space group). Since the Bravais lattice is base centered and not a primitive lattice, some care must be exercised in counting the normal modes when using multiply primitive cells. (A C lattice has twice the number of atoms as a primitive lattice.) In this paper we avoid this problem and work with a primitive cell. Also we work with the space group symmetry operations in Kovalev's book.[7]

Figure 1 shows an x,y plane projection of four base-centered unit cells. The conventional x and y axes (of the multiply primitive base-centered Bravais lattice) are labeled $\vec{a}_1$ and $\vec{a}_2$ and are, respectively, 9.63 and 5.46 Å in length. The z axis is into the paper (4.85 Å) and is called $\vec{a}_3$. The unit cell outlined in $\vec{a}_1$, $\vec{a}_2$, and $\vec{a}_3$ has twice as many atoms as the primitive cell.

Also shown in Fig. 1 are the lattice vectors of the primitive cell, $\vec{a}_i^P$, where

$$\vec{a}_1^P = \tfrac{1}{2}(\vec{a}_1 + \vec{a}_2) ,$$
$$\vec{a}_2^P = \tfrac{1}{2}(\vec{a}_2 - \vec{a}_1) , \qquad (1)$$
$$\vec{a}_3^P = \vec{a}_3 .$$

So far the origin of the multiply primitive cell and the primitive cell are at the same position as can be seen in Fig. 1. However, we also show in Fig. 1 the primitive cell displaced an amount $\vec{a}_2$ to the right. In the displaced primitive cell we have placed an origin at the center of the cell in the x-y plane (at $\frac{1}{2}\vec{a}_2$). The space group symmetry operations are taken with respect to this origin in Kovalev's book.[7]

Table I shows the atomic parameters for the atoms in[6] Li_2GeO_3 and the listings for this space group from the *International Tables for X-Ray Crystallography* for the 4*a* and 8*b* sites in fractions of the unit cell. Naturally these positions are in the normally used crystallographic unit cell (the multiply primitive base-centered cell $\vec{a}_1, \vec{a}_2, \vec{a}_3$). However, Fig. 1 also shows the atom positions with respect to the primitive cell.

In Table II we show the symmetry operations of this space group in the notations of Kovalev and in the more conventional notation. Kovalev arbitrarily uses h_i, i = 1 to 48, for the 48 possible point-group operations for the O_h ($m3m$) point group and its subgroups. In order, the symmetry operations of this space group are the identity; a twofold screw operation; a glide operation; a reflection. These operations can be readily seen in Fig. 1. Table II also lists the characters of the representation that describe the transformation of arbitrary displacements of atoms in the 4*a* and 8*b* sites when operated on by the various symmetry operations of the space group. Here we have used the atoms in the primitive cell. The right side of Table II shows the reduction of the representation according to the irreducible representations of the point group C_{2v}. This point group is isomorphic to the factor group of the space group with respect to the primitive translations. A 4*a* site is occupied

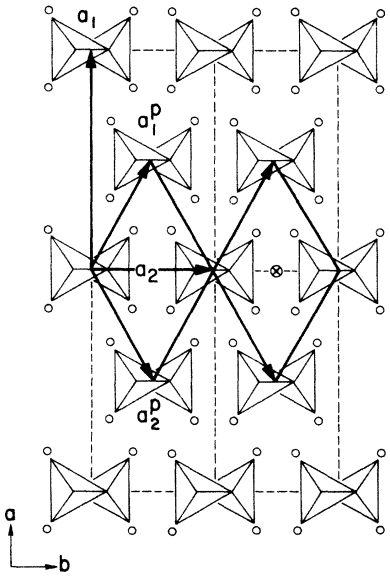

FIG. 1. View in the x-y plane of four base-centered unit cells of Li_2GeO_3.

by Ge and O(1) atoms (two of each in the primitive cell). Li and O(2) occupy 8b sites. So the total number of normal modes transform as the

$$10A_1^z + 8A_2 + 8B_1^x + 10B_2^y \quad (2)$$

irreducible representations of the point group C_{2v}. We expect that $3n$ = number of normal modes = (3) $\times$(12) = 36, where n is the number of atoms in the primitive unit cell. All the irreducible representations in C_{2v} point symmetry are one dimensional, so Eq. (2) also shows that there are 36 normal modes, all at different frequencies. The superscripts in Eq. (2) show which modes transform as z, x, and y. The acoustic modes transform as $A_1 + B_1 + B_2$, so the optic normal modes transform as $9A_1^z + 8A_2 + 7B_1^x + 9B_2^y$. The A_1, B_1, and B_2 modes

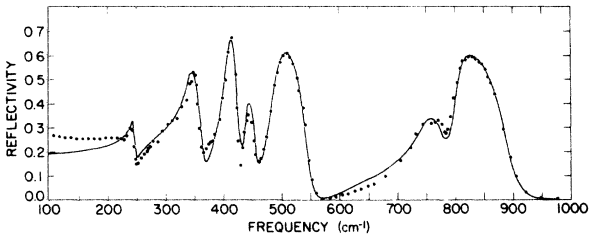

FIG. 2. Experimental ir reflectivity data for E parallel to the a axis (dots). The solid line is the best fit theoretrical curve obtained from a KK analysis of the experimental data.

are allowed in infrared measurements with the electric-field vector polarized along the z, x, and y axis, respectively. All the modes are Raman allowed.

III. EXPERIMENTAL DETAILS

A. Infrared

Polarized reflectivity measurements at room temperature on each of three orthogonal faces of a Li_2GeO_3 crystal were obtained using a Perkin Elmer model No. 301 far-infrared spectrometer. The large size of the crystal permitted one to use a 9.4-mm-diam circular area on each orthogonal face. All measurements were normalized against a gold mirror. AgCl plates stacked at Brewsters angle and a gold grid wire polarizer were used to select one polarization of the reflected infrared radiation. Data were taken over the frequency range 70–10 000 cm^{-1}.

B. Raman

The measurements were taken with a conventional laser-Raman spectrometer.[8] The A_1, B_1, and B_2 modes are infrared active, so the direction of propagation of the phonon with respect to the polar-

TABLE I. Atomic positions in Li_2GeO_3.

Space group: $Cmc2_1$ (C_{2v}^{12})			Coordinates of equivalent positions (0, 0, 0) ($\frac{1}{2}$, $\frac{1}{2}$, 0)		
Number of positions	Wykoff notation	Point symmetry			
8	b	1	(x,y,z) $(\bar{x},y,z)$ $(\bar{x},\bar{y},\frac{1}{2}+z)$ $(x,\bar{y},\frac{1}{2}+z)$		
4	a	m	$(0,y,z)$ $(0,\bar{y},\frac{1}{2}+z)$		
			Atomic parameters		
Atom	Position		x	y	z
Li	8b		0.176	0.345	0.005
Ge	4a		0	0.1787	0.5
O(1)	4a		0	0.140	0.835
O(2)	8b		0.152	0.318	0.412

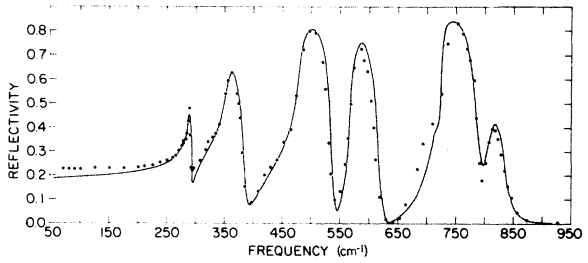

FIG. 3. Experimental ir reflectivity data (dots) for E parallel to the b axis. The solid line is the best fit theoretrical curve obtained from a KK analysis of the experimental data.

ization of the phonon is important. For the results here, we have measured only pure transverse-optic (TO) modes. This is done by realizing that the polarization (mechanical separation of charge) of an A_1 phonon is along the z axis. So if the phonon is propagated in the x-y plane, the A_1 (TO) phonon frequency is measured. We use the notation $a(bc)d$ to mean that the laser light is incident on the crystal in the a direction and polarized in the b direction and that the scattered light is polarized in the c direction and leaves the crystal in the d direction. Thus $x(zz)y$ has the phonon propagating in the x-y plane with zz polarizability which will measure phonons with A_1 symmetry in a Raman experiment. The polarization of an A_1 phonon is in the z direction. Since the phonon is propagating perpendicular to the z axis, we have TO phonons or A_1 (TO). In a similar manner B_1 (TO) and B_2 (TO) pure phonons were measured. Phonons that transform as the A_2 irreducible representation of the C_{2v} point group are not infrared active, so the direction of propagation is not important. It is only necessary to set the input (y) and the exit (x) polarizers in order to observe (yx) polarizability.

C. Index of refraction measurements

The index of refraction along each crystal axis was measured using a Zeiss Abbé refractometer. The same crystal was used for these measurements as was used for the ir reflectivity measurements. The incident light was passed through a monochromator and polarizer before entering the refractometer so that the E vector was parallel to one of the three orthogonal crystal axes during each measurement. The wavelength range of the measurements was limited to the visual region and the highest index that could be read with the available refracting prism was 1.71.

D. Dielectric-constant measurements

Dielectric-constant measurements were taken on three oriented samples. The samples typically had an area of 30 mm^2 and a thickness of 0.5 mm. Silver-painted electrodes were used for the small signal capacity measurements taken at 10 kHz and 26 mHz.

IV. RESULTS

A. Infrared results

The dots shown in Figs. 2–4 are the measured reflectivities for the electric vector of the light parallel to the a, b, and c axes, respectively. These points are a slightly smoothed average of many more data points. The measured reflectivity in the region between 1000 and 10 000 cm^{-1} shows only the usual slow rise in reflectivity, reaching a value at 1 μm of 0.075 to 0.08. The asymptotic value of the index of refraction extrapolated from the visible to 1 μm is about 1.66, which would give a reflectivity of 0.06. The somewhat higher measured value may be due to some reflection from the back face of the crystal and possibly unknown surface effects.

A Kramers-Kronig (KK) analysis of the reflectivity data was made for each polarization direction in order to obtain the complex dielectric constant $\hat{\epsilon} = \epsilon' + i\epsilon''$ as a function of the frequency ω.

From the peaks in the plot of $\epsilon''\omega$ vs ω one obtains the transverse-optic-mode frequencies ω_i. From the amplitude and width of each peak in the plot of ϵ'' vs ω, one can estimate the mode strengths A_i and the damping constants γ_i which occur in the independent oscillator model specifying the complex dielectric constant $\hat{\epsilon}$ by the relation

$$\hat{\epsilon} = \epsilon_\infty + \sum_i \frac{A_i}{\omega_i^2 - \omega^2 + i\gamma_i\omega} .$$

Given $\hat{\epsilon}$ one can calculate the reflectivity by the relation $R = |(\hat{\epsilon} - 1)/(\hat{\epsilon} + 1)|$. With the KK-analysis values of A_i, ω_i, and γ_i as starting points, we ad-

TABLE II. Character of the reducible representations of arbitrary displacements for the two different atomic positions.

Position	$\{h_1 \mid 0\}$ $\{E \mid 0\}$	$\{h_4 \mid \vec{\tau}\}$ $\{C_2^z \mid \vec{\tau}\}$	$\{h_{27} \mid \vec{\tau}\}$ $\{\sigma_v^y \mid \vec{\tau}\}$	$\{h_{26} \mid 0\}$ $\{\sigma_v^x \mid 0\}$	$\vec{\tau} = \frac{1}{2}\vec{a}_3$
$4a$	6	0	0	2	$\rightarrow 2A_1 + A_2 + B_1 + 2B_2$
$8b$	12	0	0	0	$\rightarrow 3A_1 + 3A_2 + 3B_1 + 3B_2$

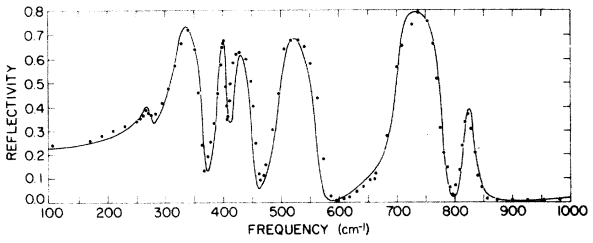

FIG. 4. Experimental ir reflectivity data (dots) for E parallel to c axis. The solid line is the best fit theoretrical curve obtained from a KK analysis of the experimental data.

justed these parameters to obtain good agreement between the experimental and calculated values of the reflectivity. In general the ω_i values changed by less than 1%. The optimum values so obtained are listed in Table III and were used to plot the solid line curve in Figs. 2–4.

B. Raman results

As mentioned in the experimental section of the ir-active modes, the transverse-optic modes A_1 (TO), B_1 (TO), and B_2 (TO) were measured by the Raman technique. The corresponding longitudinal-optic modes that transform as these irreducible representations were not measured. However, these measured modes can be compared with the infrared results where the TO modes can be obtained from analysis of the reflectivity data. Raman techniques also can be used to measure the modes that transform as the A_2 irreducible representation of the C_{2v} point group. This mode is not infrared active so a comparison can not be made.

Figure 5 shows the Raman results for these modes and Table IV lists the values of the frequencies. Considerable care and checking must be exercised when a mode is observed to be very intense in one symmetry and very weak in another symmetry, both with approximately the same frequency. The observation of the weak line can be

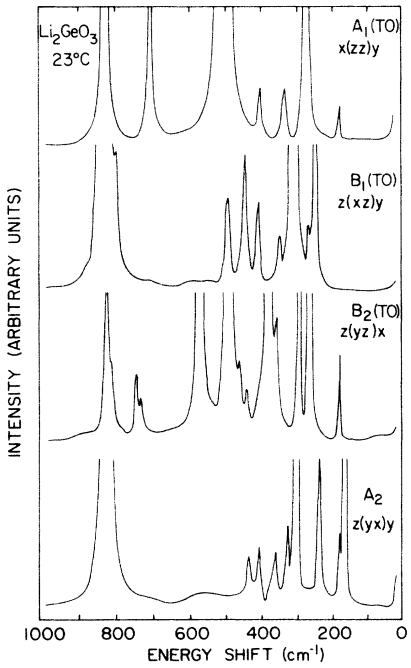

FIG. 5. Intensity of the Raman-scattered light vs energy shift from the 5145-Å exciting line.

spurious, caused by finite aperture effects. This point was carefully checked by decreasing the aperture.

C. Index-of-refraction and dielectric-constant results

Shown in Fig. 6 is the wavelength dependence of the index of refraction along each of the crystal axes. These results agree with earlier work where only an averaged index was reported.[9]

The dielectric-constant results are presented in Table V. The difference between the values at 10 kHz and 26 MHz is due to the piezoelectric response of the crystal. The measurement at 26 MHz, being above the frequency at which the crystal can respond, is for the "clamped" crystal condition and is the value to be compared with the ϵ

TABLE III. TO frequencies, mode strengths, and widths from infrared reflectivity measurements.

B_1 ($\vec{E} \parallel \vec{a}$)			B_2 ($\vec{E} \parallel \vec{b}$)			A_1 ($\vec{E} \parallel \vec{c}$)		
$10^{-3}A$	ω (cm^{-1})	α (cm^{-1})	$10^{-3}A$	ω (cm^{-1})	α (cm^{-1})	$10^{-3}A$	ω (cm^{-1})	α (cm^{-1})
120	805	22	16	802	27	23	813	13
285	755	50	105	725	5.2	220	703	11.5
120	490	215	100	715	15	120	500	17
42	444	15	90	569	9.5	50	420	15
120	409	10	300	480	12.5	70	394	7
150	344	20	170	354	16	270	322	18
15	247	9	25	288	5	39	271	17

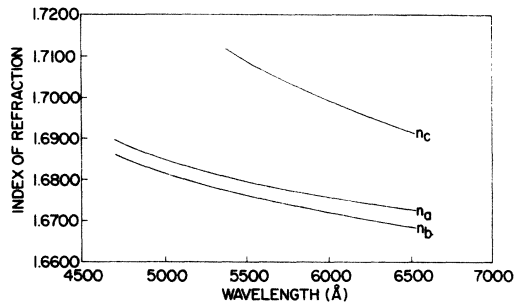

FIG. 6. Optical index of refraction vs wavelength for each of the three crystal axes.

values obtained from the ir reflectivity measurements.

V. DISCUSSION

As can be seen in Fig. 1, along the z axis there is a zigzag linkage of Ge–O–Ge–O$\cdots$ with each Ge ion surrounded by four O ions, but one oxygen atom is shared with the GeO_4 group above and one oxygen atom with the GeO_4 group below. Thus one cannot try the molecular approximation using isolated GeO_3 or GeO_4 units. Figure 1 also shows that a dipole moment per unit volume (a polarization) along the z axis is possible, i.e., the $+z$ direction is different from the $-z$ direction. However, it is also apparent that this polarization probably is not reversible because the difference in the positive and negative z directions does not stem from small displacements from a centrosymmetric structure.

From Table IV we see that except for the A_1 (TO) modes, more Raman lines are observed then the crystal symmetry allows in first order. Obviously some of these lines are due to second-order effects. In the case of the ir results, except for the B_1 (TO) modes, not enough vibrational frequencies are determined as are permitted by the symmetry of the crystal space group. Thus in order to compare the two sets of results, we must make some judgment as to which Raman modes are to be compared with the ir modes. This problem is partly resolved by the very close spacing of some of the Raman frequencies, since ir reflectivity measurements will not separate very closely spaced modes. A comparison of the two sets of results is shown in Table VI. The Raman lines with parentheses around them are so closely spaced that either or both should be compared with the adjacent ir line. In general we see that all but three of the ir frequencies agree very well with a corresponding Raman frequency and the agreement is best for the A_1 (TO) modes where there are equal number of Raman and ir lines.

TABLE IV. Frequency of observed Raman lines (cm^{-1}).

B_1(TO) $z(xz)y$	B_2(TO) $z(yz)x$	A_1(TO) $x(zz)y$	A_2 $z(yx)y$
817	818	822	820
796	806	699	434
495	742	501	406
447	729	401	360
407	570	333	325
349	493	267	297
305	461	177	234
268	440		177
247	381		158
	358		
	292		
	262		
	177		

TABLE V. Values of the dielectric constant. $\epsilon_\infty = 2.6$.

	$\vec{E} \parallel \vec{a}$	$\vec{E} \parallel \vec{b}$	$\vec{E} \parallel \vec{c}$
ϵ (10 kHz)	7.8	8.6	13.6
ϵ (26 MHz)	5.6	6.7	10.9
ϵ (mode)	6.4	6.5	7.6

In Table V, in the row labeled ϵ (mode), we have listed values of the zero-frequency dielectric constant calculated from the ir results using the expression

$$\epsilon(0) = \epsilon(\infty) + \sum \frac{A_i}{\omega_i^2} .$$

The results are in reasonable agreement with the measured clamped dielectric constant except for the c-axis result, which is significantly low.

TABLE VI. Comparison of Raman- and ir-determined modes (cm^{-1}).

B_1(TO)		B_2(TO)		A_1(TO)	
ir	Raman	ir	Raman	ir	Raman
805	(817, 796)	802	(816, 806)	813	822
				703	699
755			742	500	501
490	495	725	729	420	
444	447	715		394	401
409	407	569	570	322	333
344	349		(493, 461)	271	267
	305	480			177
	268		440		
247	247		381		
		354	358		
		288	292		
			262		
			177		

ACKNOWLEDGMENTS

We would like to express our appreciation to Louis Manganaro and Frank Dacol for their excellent assistance in helping to take and analyze much of the experimental data, and Dr. B. Scott for providing the single crystals that were used.

---

*Partially supported by the U. S. Army Research Office, Durham, N. C.

[1]B. A. Scott, K. A. Ingebrigtsen, and C. S. Tseng, Mater. Res. Bull. 5, 1045 (1970).
[2]A. Grund and M. Pizy, Acta Crystallogr. 5, 837 (1952).
[3]H. Seeman, Acta Crystallogr. 9, 251 (1956).
[4]Y. Ginetti, Bull. Soc. Chim. Belg. 63, 460 (1954).
[5]H. Hahn and U. Theune, Naturwissenschaften 44, 33 (1957).
[6]H. Völlenkle and A. Wittmann, Monatsh. Chem. 99, 244 (1968).
[7]O. V. Kovalev, *Irreducible Representations of the Space Groups* (Gordon and Breach, New York, 1965).
[8]G. Burns and B. A. Scott, Phys. Rev. B 7, 3088 (1973).
[9]A. N. Lazarev and T. F. Tenisheva, Opt. Spectrosc. 13, 708 (1962).